Geophysical Research Letters
NOV 8 2006; 33 (21) NIL_11-NIL_15
http://dx.doi.org/10.1029/2006GL027335

An edited version of this paper was published by AGU.

New structural and geochemical observations from the Pacific-Antarctic Ridge between 52°45′S and 41°15′S

F. Klingelhoefer[,1] H. Ondréas[,1] A. Briais[,2] C. Hamelin[,3] and L. Dosso[4]

1Department of Marine Geosciences, IFREMER, BP70, 29280 Plouzané, France.
2CNRS, UMR 5562, OMP, 14, Ave. E. Belin, 31400 Toulouse, France
3IUEM/UBO, Place Copernic, Plouzané, France.
4CNRS, UMR 6538, Domaines Océaniques, BP 70, 29280 Plouzané, France.

Abstract:

We investigated the morphology and structure of the Pacific-Antarctic Ridge between 52°45′S and 41°15′S during the Pacantarctic2 cruise using multibeam echosounder together with gravity measurements and dredges. Analysis of the bathymetric, gravity and geochemical data reveal three ridge segments separated by overlapping spreading centers south of the Menard transform fault (MTF) and five segments north of it. Calculation of the cross-sectional area allows quantification of the variation in size of the axial bathymetric high. Together with the calculation of the mantle Bouguer anomaly, these data provide information about variations in the temperature of the underlying mantle or in crustal thickness. Areas with hotter mantle are found north and south of the MTF. Geochemical analyses of samples dredged during the survey show a correlation of high cross-sectional area values and negative mantle Bouguer anomalies in the middle of segments with relatively less depleted basalts.

1. Introduction

The medium-fast spreading Pacific-Antarctic Ridge in the southern Pacific has been much less explored than the fast-spreading East Pacific Rise or the slow-spreading Mid-Atlantic Ridge, mainly because of its remoteness. First seafloor bathymetric data revealed the absence of the predicted axial rift [Menard, 1990] and together with magnetic traverses allowed to image the geometry of spreading segments and transform faults [Molnar *et al.*, 1975, Weissel *et al.*, 1977]. The first full sonar coverage of this part of the ridge crest between 57^{o}S and 34^{o}S was achieved in 1991 [Lonsdale, 1994]. The southernmost parts of the Pacific-Antarctic Ridge were surveyed by Cande *et al.* [1995] and Géli *et al.* [1997]. Along this ridge, geochemical sampling was carried out south of 52^{o}S [Géli *et al.*, 1997, Natland *et al.*,1992, Castillo *et al.*, 1998] and north of 42^{o}S only [Stoffers *et al.*, 2001, Haase *et al.*, 2005].

The morphology of a spreading axis depends strongly on the spreading rate. Slow-spreading ridges, with half spreading rates less than 12 mm/yr, are generally characterized by a prominent axial valley, while fast-spreading ridges, with rates faster than 80 mm/yr, exhibit a smooth triangular morphology with an axial high [Macdonald, 1986]. In the study area, half spreading rates vary from 46 mm/yr in the south to 50 mm/yr in the north [DeMets *et al.*, 1990] and most of the ridge in this region shows an unrifted crest typical of fast-spreading ridges [Lonsdale, 1994]. From bathymetric and side-scan sonar data, Lonsdale [1994] proposed that the segmentation pattern of this section of the Pacific-Antarctic Ridge results from its kinematic history rather than from 3-D mantle upwelling.

2. Data Acquisition

During the Pacantarctic 2 cruise (Figure 1), gravimetric data were acquired using a BGM5 gravimeter, which offers a precision between 0.4 and 1.6 mGal depending on the state of the sea, and an instrument drift less than 2 mGal per month. The data were corrected for the instrument drift and the Eötvös correction was applied to allow the calculation of the free-air anomaly. A SIMRAD EM12 multibeam system was used to collect bathymetry and backscatter data along 14 to 16 km-wide swaths. The relative precision of the bathymetric data is 0.5% which corresponds to 5 meters in 2000 m water depth.

3. Bathymetry and Cross-Sectional Area

The ridge axis generally deepens from south to north in the whole study area (Figures 2 and 3 (a) and (b)). We confirm the existing interpretation of the plate boundary geometry [Lonsdale, 1994] and identify three ridge segments south of the Menard Transform Fault (MTF) and five segments north of it, separated by overlapping spreading centers [Ondreas *et al.*, 2005] (Figure 1). The morphology of the ridge axis changes from a pronounced dome (Figure 2 (a)) in segment S1, to a rifted axial high in S2 (Figure 2 (b)), and back to a very robust dome morphology in S3 (Figure 2 (c)). North of the MTF, the ridge axis changes from pronounced to less robust dome morphology from segments N1 to N3 (Figure 2 (d-f)). Segment N4 is characterized by a small summital graben (Figure 2 (g)). The ridge axis deepens and narrows along segment N5 (Figure 2 (h)) [Ondreas *et al.*, 2005, Dosso *et al.*, 2005].

Estimates of the cross-sectional area allow a quantification of the variation in size of the axial bathymetric high along the ridge axis [Scheirer and MacDonald, 1993, Pardee *et al.*, 1998]. The larger swath width used in our study compared to older studies [Lonsdale, 1994] allows for the first time the calculation of the cross-sectional area along the complete ridge axis in the study region. It provides information about the inflation of the ridge and therefore its magmatic-tectonic state. The bathymetric data from this study have been compiled onto a 200 m grid, from which the cross-sectional area was calculated automatically along the digitized ridge axis. The cross-sections are calculated at 1 km intervals, along profiles perpendicular to the axis, with a half width of 8 km (Figure 3 (c) and (d)). The cross-sectional area is then defined to be the area of the ridge above a

reference depth given by the average depth of 0.5 m.y.-old oceanic crust [Mueller *et al.*, 1997] in the region, 2750m in our study area. Areas in the direct vicinity of the MTF were excluded.

4. Gravity and Mantle Bouguer Anomaly

The free-air gravity anomaly along the ridge axis (Figure 3 (e) and (f)) is characterized by pronounced highs of up to 28 mGal over segments S1 and S3, with a low over the less robust segment S2. In the northern area the free-air anomaly generally decreases from 25 mGal at N1 to 12 mGal at N5. Discontinuities between individual segments are marked by relative gravity lows of 5 to 10 mGal.

The mantle Bouguer anomaly (MBA) was calculated by subtracting from the measured free-air gravity anomaly the gravity anomaly predicted using the method of [Parker, 1972] from a model comprised of the water-seafloor interface and a Moho interface assuming a constant density and thickness crustal model. The MBA is then interpreted to reflect anomalous crust or mantle temperatures or crustal thickness. To calculate the MBA, the bathymetric data were projected onto a Cartesian grid of 512 x 512 cells of 1.3 x 2.5 km size. Where no shipboard data were available, the bathymetry predicted from satellite altimetry [Smith and Sandwell, 1997] was used to avoid large side effects. The resulting grid was folded in x and y direction to minimize the artificial edge effect in use of Fast Fourier Transform (FFT) which assumes periodicity of the data. The crustal thickness was defined to be a constant 7 kilometers and the density of the crust and mantle were taken to be 2700 kg/m^3 and 3300 kg/m^3, respectively. As the gravity anomaly derived from satellite measurements does not provide sufficiently precise data along the axis, the mantle Bouguer anomaly was calculated from the three-dimensional predicted gravity anomaly substracted from the shipboard measurements on the shiptracks along the mid-ocean ridge only (Figure 3).

5. Geochemistry

24 dredges were collected along axis at regular intervals (Figure 1). They brought back fresh basalts which in many cases present a few cm thick glass rims. Only one dredge immediately south of MTF brought back andesitic basalts. The great majority of samples are depleted as shown by their $(Nb/Zr)_N$ ratios of less than 0.5 (Figure 3 i and j). The least depleted samples are found in ridge segments S2 and N2, as well as in segment S3, which appears to be influenced by the nearby seamount activity. Within each segment, the most depleted sample is found at the northern end, where the ridge dome becomes narrower. At the ridge section scale, the ridge becomes deeper towards the north. This northward deepening of the ridge axis is accompanied by a general decrease of $(Nb/Zr)_N$ (Figure 3).

6. Results and Discussion

The bathymetric, gravimetric and geochemical data in this study area reveal a general trend from a robust ridge with a large axial dome in the south to a less robust ridge characterized by a narrower axis with an axial graben in the north. First and second-order discontinuities cause bathymetric lows marked by low cross-sectional area values. Higher mantle Bouguer anomaly values at the discontinuities are interpreted to reflect anomalously thin crust or low mantle temperatures, in good agreement with low $(Nb/Zr)_N$ values observed in the vicinity of the discontinuities. Although the axial depth remains nearly constant along most of the segments, the cross-sectional area is larger in most segment centers, due to a broader axial dome in the middle of the segment. We infer that these variations reflect the presence of a hotter underlying mantle in the middle of the segments compared to their ends. The cross-sectional area estimates provide useful additional information to the axial depth as analysed in previous studies [Lonsdale, 1994]. The mantle Bouguer anomaly often shows a negative low in the segment center, and appears to be associated to relative mantle enrichment, with higher $(Nb/Zr)_N$ values in the segment centers. These two observations also confirm, that the middle of most segments is magmatically more active than the segment ends as proposed for the East Pacific Rise [Macdonald *et al.*, 1988]. Supposing that the small offsets of plate age at overlapping spreading centers bounding the segments do not allow for sufficient cooling to substancially decrease the mantle temperature, the fact that the middle of the segments are magmatically more roboust confirms the theory that the magmatic and thermal budget

must be controlled by processes at depth beneath each segment [Macdonald *et al.*, 1988], rather than by its kinematic history.

The segments neighbouring the Menard TF, N1 in the north and S3 to the south, show all characteristics of magmatically highly robust segments. The shallowest axial depth values of only 2250 m measured during the survey were found on segment S3, while segment N1 displays a slightly shallower axial depth of 2350 m. The cross-sectional area displays maximum values of 5.9 km^2 in the middle of S3 and 5 km^2 in the middle of N1. These bathymetric features are accompanied by negative mantle Bouguer anomaly values of -7 mGal on S3 and -5 mGal on N1. The maxima of the cross-sectional area correlate with the minima of the mantle Bouguer anomaly. All these observations indicate an abundant magma supply beneath S3 and N1 segments, suggestive of a hot underlying mantle, located north and south of MTF. This symmetry of magmatic roboust segments north and south of a transform fault is not common on the East Pacific Rise, where most fracture zones are bounded by magma starved segments or different type segments, as for example Clipperton Fracture Zone [Macdonald *et al.*, 1988].

Neighbouring these robust segments, two anomalously deep segments were observed N2 to the north and S2 to the south. The S2 segment is characterised by a small axial high and the deepest axial depth of 2650 m found during the survey. It is also the shortest segment in this region with a 100 km length. It shows an increasing cross-sectional area from 0 to 2.5 km^2 from south to north at constant axial depth. A correlative increase is also observed in the $(Nb/Zr)_N$ values of dredge samples in this segment, which indicates a decreasingly depleted mantle source towards the north. In good agreement with this,

the mantle Bouguer anomaly shows decreasing values towards the north. The segment N2 is only 110 km long. It is characterized by a small axial dome, large axial depth of 2550 m and cross-sectional area values smaller than on N1. The mantle Bouguer anomaly shows negative values comparable to that on N1. These observations indicate that the S2 and N2 segments are magmatically less robust than S3 and N1. However, the geochemical analysis of samples from the dredge located in segment N2 and to a lower degree on S2 show elevated $(Nb/Zr)_N$. Along-axis observations alone cannot explain the $(Nb/Zr)_N$ contents of the dredge samples on this segment. Possible causes may be related to the two volcanic seamount chains which intersect the ridge axis near S2 and N2. Both chains obliquely join the Menard Fracture Zone (Figure 1). The influence of the off-axis volcanism might also explain the increase in MBA along N1.

South of S2 and north of N2, the anomalous segments, two magmatically robust segments S1 and N3 are observed (Figure 3). S1 is characterized by an axial depth around 2400 m and a broad axial dome, leading to high cross-sectional area values up to 4 km^2. The cross-sectional area is largest in the middle of the segment while the seafloor depth remains nearly constant along most of the segment. The mantle Bouguer anomaly shows a minimum in the segment center and geochemical sampling indicates a more depleted mantle than in the anomalous segments S2 and N2 and highest values in the segment center. Segment N3 shows a slightly larger axial depth (2500 m) and higher mantle Bouguer anomaly than S3. Again the least depleted geochemical samples are found in the segment centers. These observations are thus confirming the description of two robust segments with hotter underlying mantle material in their centers.

Segments N4 and N5 show a gradual increase in axial depth, however the cross-sectional area decreases 1 km^2 along N4 and increases again along N5, indicating that the thermal state of the underlying mantle changes along these segments, with a hotter mantle in the northern half of the segment N5 (Figure 3). This is confirmed by the MBA which shows an increase along N4 and decreases along N5 possibly caused by hot underlying mantle. Geochemical analyses of samples along these segments however do not reflect these changes but show a constant decrease of the $(Nb/Zr)_N$ ratio following the axial depth values. Samples from an off-axis volcanic ridge near segment N5 show $(Nb/Zr)_N$ ratios comparable to basalts dredged on N5.

7. Conclusions

The Pacific-Antarctic ridge between 52^{o}45'S and 41^{o}15'S is characterized by a gradual increase of axial ridge depth and a decrease of the cross-sectional area. The morphology of the central high changes from a broad dome to a narrow high with a small summittal graben. Most segments show cross-sectional area maxima, mantle Bouguer minima and least depleted geochemical characteristics in their middle, supporting the theory that the axial magmatic and thermal budget depends on processes at depth beneath each segment [Macdonald *et al.*, 1988]. Both segments immediately south and north of MTF (S3 and N1) are characterized by less depleted basalt chemistry than other segments in this region, shallow axial depth, high cross-sectional area values and negative MBA values, an observation which is uncommon in the vicinity of fracture zones. The neighbouring segments (S2 and N2) are anomalously deep and show elevated $(Nb/Zr)_N$ values. These observations may be related to the presence of two off-axis volcanic seamount chains intersecting the ridge axis between these robust and anomalous segments and obliquely joining the fracture zone. Bordering these anomalous segments are again magmatically robust segments (S3 and N3). The northernmost segment N5 has a deep axial valley, but low MBA values which could indicate hot underlying mantle or large crustal thickness.

Acknowledgments. We thank the captain and the crew of the N/O Atalante for their help in the data acquisition. We also thank L. Matias for help in mantle Bouguer calculations. The GMT [Wessel and Smith, 1995] software was used for several figures. We would also like to thank two anonymous reviewers for valuable comments on the original manuscript.

References

Cande, S. C., C. A. Raymond, J. Stock, and W. F. Haxby (1995), Geophysics in the Pitman Fracture Zone and Pacific Antarctic Plate motions during the Cenozoic, *Science 270*, pp. 947–953.

Castillo, P. R., J. Natland, Y. Niu, and P. F. Londsdale (1998), Sr, Nd and Pb isotopic variation along the Pacific-Antarctic risecrest, 53-57^{o}s: implications for the composition and dynamics of the South Pacific upper mantle., *Earth Planet. Sci. Lett., 154*, pp. 109–125.

DeMets, C., R. G. Gordon, D. F. Argus, and S.Stein (1990), Current plate motions, *Geophys. J. Inter. 101*, pp. 425–478.

Dosso, L., H. Ondréas, and the Pacantarctic 2 Shipboard Scientific Party (2005), Geophysical survey and geochemical sampling of the Pacific-Antarctic Ridge between 41^{o}15s and 52^{o}45s: initial results of the pacantarctic 2 cruise, *Interridge, 14*, pp. 1–4.

Géli, L., et al. (1997), Evolution of the Pacific-Antarctic Ridge south of the Udintsev Fracture Zone, *Science 278*, pp. 1281–1284.

Haase, K. M., N. A. Stroncik, R. Hékinian, and P. Stoffers (2005), Nb-depleted andesites from the Pacific-Antarctic Rise as analogues for early continental crust, *Eos Trans. AGU, 86(52)*, pp. V41C–1460.

Lonsdale, P. (1994), Geomorphology and structural segmentation of the crest of the southern (Pacific-Antarctic) East Pacific Rise., *J. Geophys. Res., 99 (B3)*, pp. 4683–4702.

Macdonald, K. C. (1986), The crest of the Mid Atlantic Ridge: Models for crustal generation and tectonics, *in: The western North Atlantic region (Vogt, P. R. ed.), Boulder,*

Colorade, Geol. Soc. Am., Geology of North America v. M, pp. 51–68.

Macdonald, K. C., P. J. Fox, L. J. Perram, M. F. Eisen, R. M. Haymon, S. P. Miller, S. M. Carbotte, M.-H. Cormier, and A. N. Shor (1988), A new view of the mid-ocean ridge from the behaviour of ridge-axis discontinuities, *Nature, 335*, pp. 217–224.

Menard, H. W. (1990), Developement of median elevations in ocean basins., *Bull. Geol. Soc. Am. 69*, pp. 1179–1186.

Molnar, P. T., T. Atwater, J. Mammerickx, and S. Smith (1975), Magnetic anomalies, bathymetry, and the tectonic evolution of the South Pacific since the Late Cretaceous., *Geophys. J. R. Astron. Soc., 40*, pp. 383–420.

Mueller, R. D., W. R. Roest, J.-Y. Royer, L. M. Gahagan, and J. G. Sclater (1997), Digital isochrons of the world's ocean floor, *J. Geophys. Res. 102 (B2)*, pp. 3211–3214.

Natland, J. H., Y. Niu, P. R. Castillo, R. F. Lonsdale, and S. H. Bloomer (1992), Petrologic exploration of the Pacific-Antarctic East Pacific Rise in the vicinity of the Udintsev and Eltanin transform faults., *Eos Trans. Am. Geophys. Union 75*, p. 742.

Ondréas, H., F. Klingelhoefer, A. Briais, C. Hamelin, and L. Dosso (2005), The Pacific-Antarctic Ridge between 41^{o}S: hot underlying mantle evidenced by bathymetry and gravity studies coupled to geochemical results., *EOS Transaction, 86*, p. 52.

Pardee, D. R., R. N. Hey, and F. Martinez (1998), Cross-sectional areas of mid-ocean ridge axes bounding the Easter and Juan Fernandez microplates, *Mar. Geophys. Res. 20*, pp. 517–531.

Parker, R. L. (1972), The rapid calculation of potential anomalies, *Geophys. J. R. astr. Soc. 31*, pp. 447–455.

Scheirer, D. S., and K. C. MacDonald (1993), Variation in cross-sectional area of the axial ridge along the East Pacific Rise: Evidence for the magmatic budget of a fast spreading center, *J. Geophys. Res. 98 (B5)*, pp. 7871–7885.

Smith, W., and D. Sandwell (1997), Global seafloor topography from satellite altimetry and ship depth soundings, *Science 277*, pp. 1956–1962.

Stoffers, P., T. Worthington, R. Hkinian, S. Petersen, M. Hannington, and M. Trkay (2001), Silicic vocanism and hydrothermal activity documented at pacific-antarctic ridge, *Eos Trans. Am. Geophys. Union 83*, pp. 301–304.

Weissel, J. K., D. E. Hayes, and E. M. Herron (1977), Plate tectonic synthesis: The displacements between Australia, New Zealand and Antarctica since the Late Cretaceous, *Mar. Geol., 25*, pp. 231–277.

Wessel, P., and W. H. F. Smith (1995), A new version of the Generic Mapping Tool (GMT), *EOS, Trans. Am. Geophys. Un., 76*, p. 329.

8. Figure Captions

Figure 1: Seafloor bathymetry of the study region. Grid represents the shipbord data and contours predicted bathymetry from satellite altimetry [*Smith and Sandwell*, 1997]. Ship navigation is marked by a black line and dredge locations by black dots. Inset shows location of the study area. Black lines are plate boundaries.

Figure 2: Multibeam bathymetry from side scan sonar data for representative parts of all ridge segments in the study area.

Figure 3: (A) Axial depth south of Menard TZ from multibeam bathymetry data (B) Axial depth north of Menard TZ (C) Cross-sectional area along the ridge axis south of Menard TZ (D) Cross-sectional area along the ridge axis north of Menard TZ (E) Free-air gravity anomaly from shipboard measurements along the ridge axis south of Menard TZ. (F) Free-air gravity anomaly from shipboard measurements along the ridge axis north of Menard TZ. (G) Mantle Bouguer anomaly from 3D calculations along the ridge axis south of Menard TZ (H) Mantle Bouguer anomaly along the ridge axis north of Menard TZ (I) $(Nb/Zr)_N$ ratio from dredges south of Menard TZ. (J) $(Nb/Zr)_N$ ratio from dredges located north of Menard TZ.

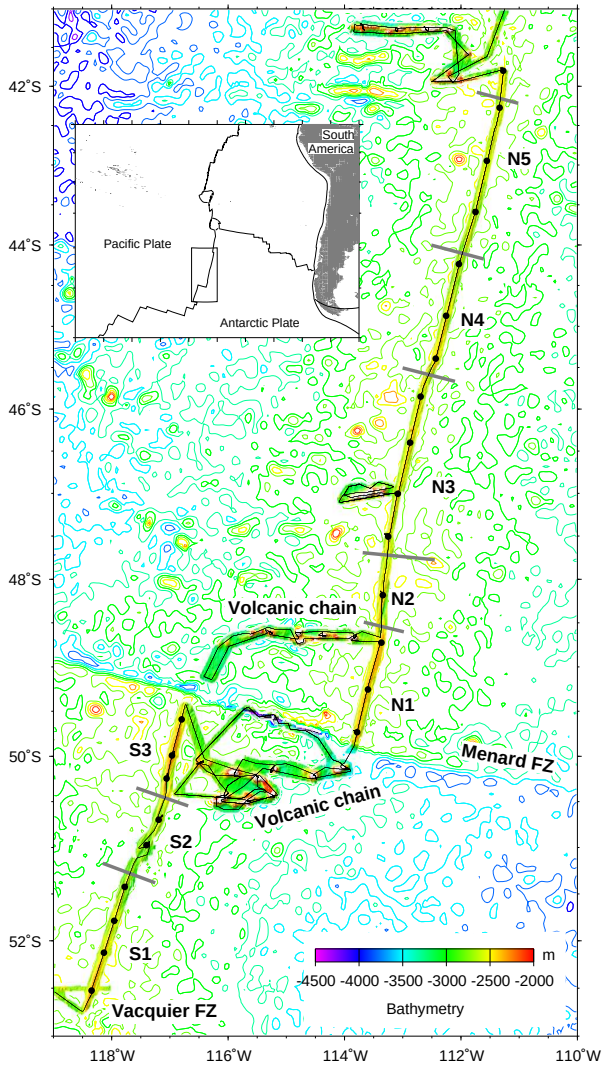
42°S
44°S
46°S
48°S
50°S
52°S
118°W
116°W
114°W
112°W
110°W
South America
Pacific Plate
Antarctic Plate
N5
N4
N3
N2
N1
Volcanic chain
Menard FZ
Volcanic chain
S3
S2
S1
Vacquier FZ
m
-4500 -4000 -3500 -3000 -2500 -2000
Bathymetry

Figure 1.

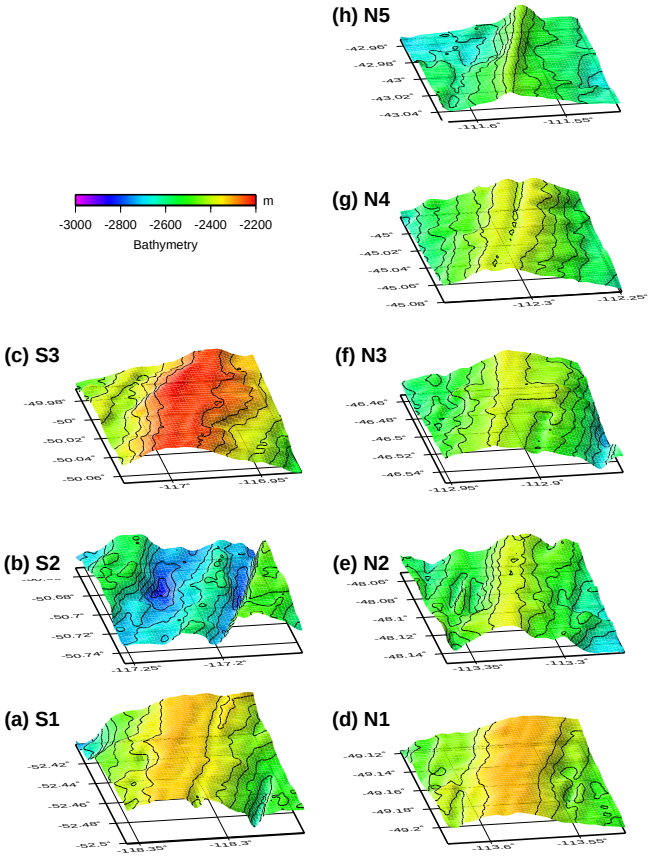
(h) N5
(g) N4
m
-3000 -2800 -2600 -2400 -2200
Bathymetry
(c) S3
(f) N3
(b) S2
(e) N2
(a) S1
(d) N1

Figure 2.

-

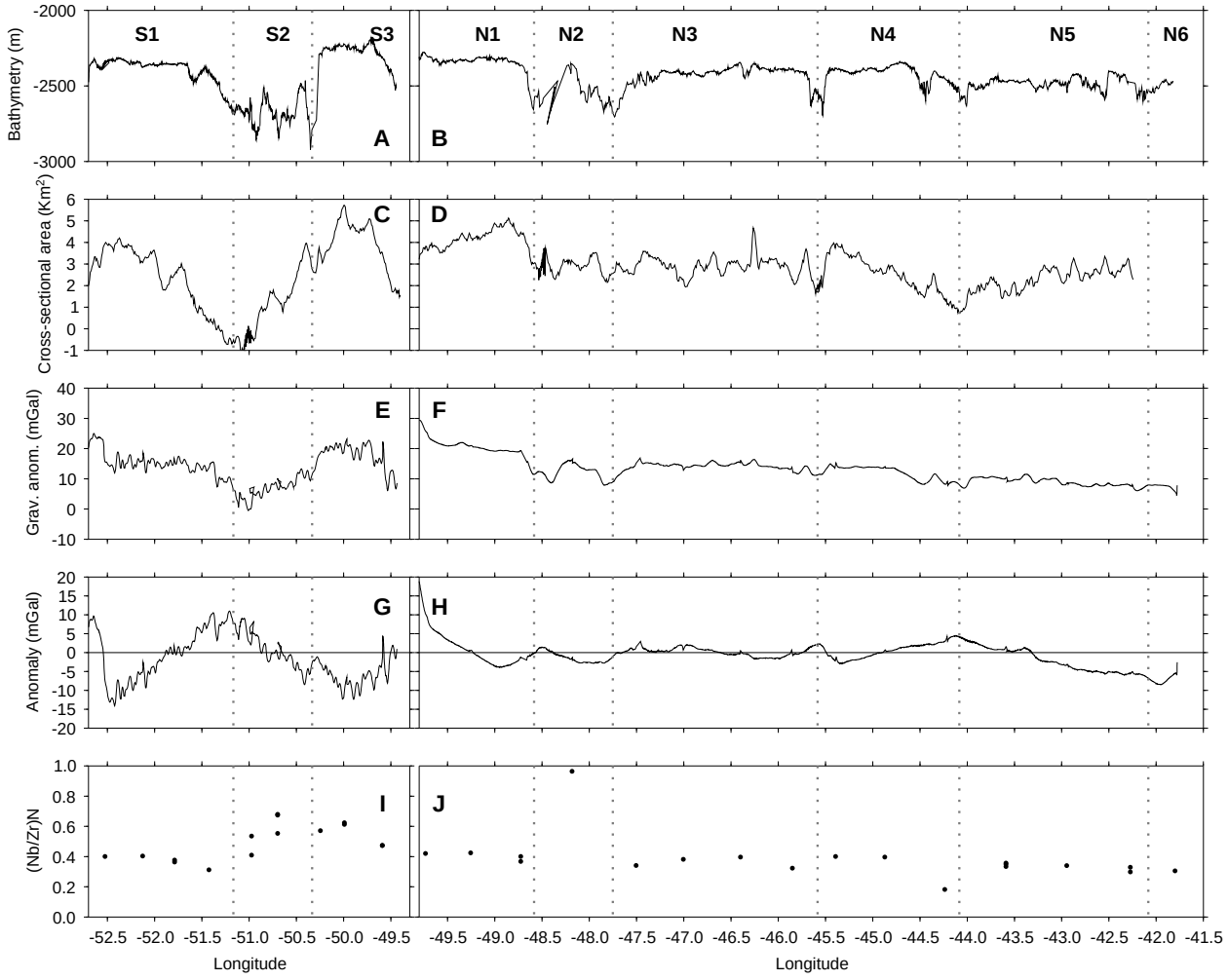
S1
S2
S3
N1
N2
N3
N4
N5
N6
A
B
C
D
E
F
G
H
I
J
Bathymetry (m)
Cross-sectional area (Km²)
Grav. anom. (mGal)
Anomaly (mGal)
(Nb/Zr)N
Longitude
Longitude

Figure 3.